Mg II absorber clustering along QSO sightlines

A project report
submitted in partial fulfillment for the award of the dual-degree of
Bachelor and Master of Science
in
Physics
by

H S Sunil Simha

under the guidance of
Dr. L. Sriramkumar, IIT Madras
Dr. R Srianand, IUCAA, Pune

Department of Physics
Indian Institute of Technology Madras
Chennai 600036, India

April 2018

CERTIFICATE

This is to certify that the project titled **MgII absorber clustering along QSO lines of sight** is a bona fide record of work done by **H S Sunil Simha** towards the partial fulfillment of the requirements of the Master of Science degree in Physics at the Indian Institute of Technology, Madras, Chennai 600036, India.

(L. Sriramkumar, Project supervisor)

ACKNOWLEDGEMENTS

I would take this opportunity to thank IIT Madras and IUCAA for providing me with this opportunity to work on this research project. I am grateful to **Dr. L. Sriramkumar** and **Dr. R Srianand** for their constant guidance and motivation even with their extremely busy schedules and research of their own. I would also like to thank the makers of the **halotools** and **hmf** libraries in Python which made my life that much more simple in obtaining the correct forms of the NFW profile and the halo mass function efficiently. Lastly, a fervent thank you to the makers of **Jupyter notebooks** where I tested all my code and obtained results.

ABSTRACT

The 279.6-280.3 nm MgII absorption doublet is found ubiquitously in spectra of distant quasars. These arise in intervening clouds found mostly in the circumgalactic medium of galaxies. With the huge number of these absorbers found and catalogued from SDSS, it is possible to study the distribution of these absorbers along lines of sight of quasars. In this study, I attempt to use a previously suggested model of gas distribution in dark matter halos to reproduce the observed number density of absorbers in redshift space. Specifically, I attempt to find the ranges of halo masses that contribute to absorption at different redshifts between 0.3 and 2.5.

Contents

Chapter 1

Introduction

1.1 Mg II absorbers along QSO sightlines

In the last few decades, there has been a growing number of spectroscopic surveys that have targeted extremely distant and extremely faint objects. Specifically, the Sloan Digital Sky Survey (SDSS) has uncovered violently luminous quasi-stellar-objects (QSOs) or quasars at high redshifts. Upon inspecting these spectra, one finds absorption lines occurring at various frequencies. Chiefly, metal ions like Mg+, Fe+ and Si+ [6] from intervening gas clouds (fig. 1.1) have been found to be ubiquitous in these spectra. Mg II absorption systems are

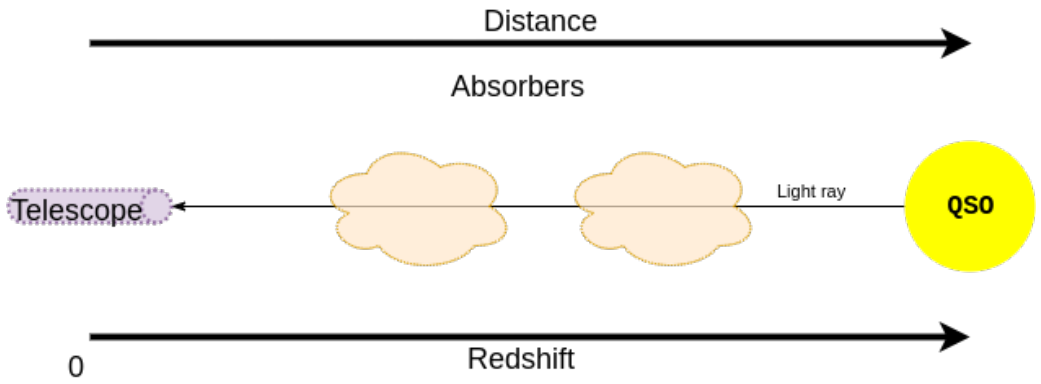

Figure 1.1: QSOs serve as background continuum sources whose light passes through gas clouds. Systems of absorption lines are imprinted upon the spectrum at various redshifts and are detected in spectrometers attached ot telescopes.

known tracers of neutral gas [2][12] and have been found to be associated with the circumgalactic medium of luminous galaxies [1][15]. Thus, one can indirectly trace out halos of

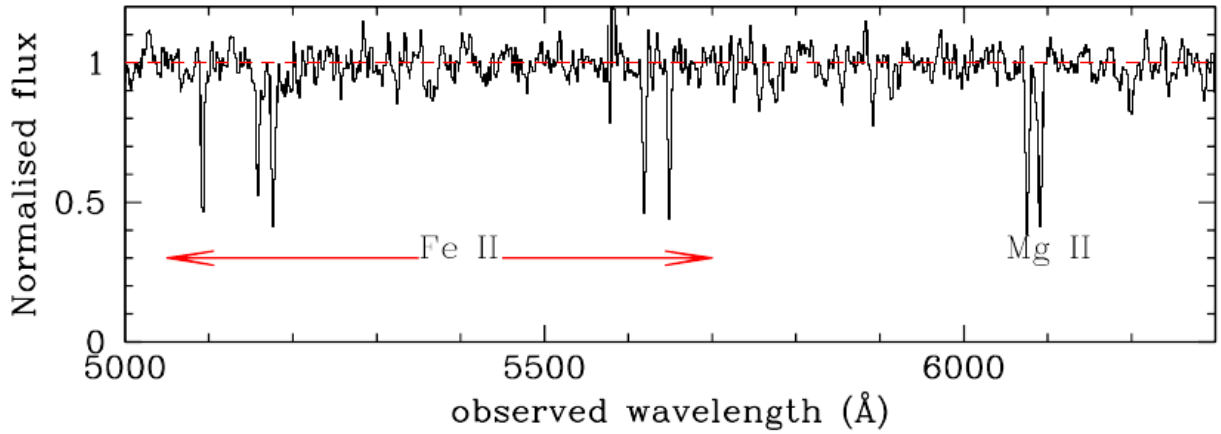

bb

Figure 1.2: A typical continuum normalised spectrum observed by the SDSS. Note the metal ion absorption lines occur at wavelengths very different from their rest frame values because of the cosmological expansion. *Source: R. Srianand, private communication*

dark matter by looking at these absorbers. In particular, the Mg II $279.6 - 280.3$ nm doublet is of particular interest to the observational community because of its components' large oscillator strengths and ubiquity. It is commonly seen in visible and infra-red parts of the spectrum (fig. 1.2) at redshifts of 0.3-2.5 and thus are popular tools for tracing out gas distribution around galaxies in that redshift space. The aim of this project is to understand through modelling the distribution of gas in dark matter halos. Tinker and Chen in their 2008 paper [16] (henceforth TC08) developed models to explain the observed number density of absorbers and the galaxy-absorber bias. This project takes the so-called Classical Model from their work and tries to find model parameters that can explain the observed number density of absorbers in the Zhu-Menard catalogue [19]. Specifically, the aim is to find the ranges of halo masses that contribute to absorption at each redshift.

This manuscript is thus split into the following sections: Chapter 2 talks about the theory of cosmological perturbations and formation of structure. This is necessary to understand the process of halo formation. Chapter 3 discusses the Press-Schechter formalism and corrections to it so as to understand the number density of halos in a given mass range. Chapter 4 describes the data catalogue. Chapter 5 describes the gas distribution model in halos as proposed in TC08 and finally concludes with the results obtained.

Chapter 2

Cosmological perturbation theory*

2.1 Introduction

One of the successes of the general theory of relativity is the explanation of the cosmological expansion of the universe and the subsequent inference that there was the Big Bang, an event of unimaginable proportions that "started" the universe. General relativity could describe cosmological evolution if one could determine the matter distribution of the universe. In the days before computers, it was very difficult to solve the Einstein equations for a general case. This did not stop the development of solutions for certain special cases. The uniform, isotropic universe gives rise to the Friedmann-Lemaitre-Robertson-Walker (FLRW) metric and subsequently one obtains the Friedmann equations for the evolution of the universe, specifically, the scale factor $a(t)$. The first Friedmann equation is

$$\begin{aligned} H^2 &= H_0^2 \left[\frac{\Omega_{m0}}{a^3} + \frac{\Omega_{r0}}{a^4} + \Omega_{\Lambda 0} + \frac{1-\Omega_0}{a^2} \right] \\ \frac{\ddot{a}}{a} &= -\frac{H_0^2}{2}[\frac{3P}{\rho_{cr_0}} + \Omega] \end{aligned} \tag{2.1}$$

Where H is the Hubble parameter, $\Omega_m, \Omega_r, \Omega_\Lambda$ represent the energy densities in units of the critical density ($\rho_{cr_0} = 3H_0^2/8\pi G$) of non-relativistic matter, relativistic matter and the cosmological constant and $\Omega = \Omega_m + \Omega_r + \Omega_\Lambda$. The subscripts of 0 indicates the parameters have been measured at present time.

Observations indicate the universe is indeed homogeneous and isotropic on scales larger than 100 Mpc. This was fortuitous because then the Friedmann equations could be used

*This chapter is based on the books by Peebles[10] and Padmanabhan [9] on struture formation in the universe

successfully to describe evolution on such scales. However, on much smaller scales we do see a lot of inhomogeneity and this requires a different metric. Again, it is possible to numerically obtain solutions but they are very difficult indeed. Fortunately, observations come to our rescue here too.

The cosmic microwave background radiation (CMBR) provides very strong evidence for the big bang model. The CMBR is isotropic to very large extent and the quadrupole anisotropies have amplitudes of the order of 10 μK as compared to the monopole term of 2.7 K. This means the universe started out with very small anisotropies and thus one can hope to explore a perturbative approach to describe structure formation in the universe.

2.2 Perturbation theory in the Newtonian Limit

What one would do next would be to write down a perturbed metric in presence of a perturbed energy density and proceed to solve Einstein's equations order by order. This process is complicated by the fact that a general coordinate transformation can make the energy density field arbitrarily large or small. One can work in a specific, presumably physically well-motivated gauge and solve for all quantities or alternatively, work in a gauge with simplified equations but make it extremely hard to interpret physically.

Given these seemingly unattractive alternatives, the desperate undergraduate like myself is tempted to look for a third. Enter the world of Newtonian perturbation. One needs to keep in mind that the cosmological structures in mind (like galaxies or clusters) are well within the Hubble radius ($H^{-1} = 1/100hMpc$) the radius of a causally connected sphere in the universe, and thus cannot be expected to be affected greatly by perturbations in length-scales larger than the Hubble radius. It is only for these larger lengthscales that general relativistic effects become important. For within the hubble radius, one can use Newtonian perturbation theory without worrying about the concerns of the previous paragraph because the Newtonian limit defines a unique frame. This also simplifies the equations and makes it easy to study order by order.

2.2.1 The Newtonian Lagrangian

First we need to define a couple of quantities. Firstly, we need to define our coordinate system. There is the physical coordinate system where each position is defined by a position

vector $\mathbf{r}$ and the comoving coordinates $\mathbf{r} = a\mathbf{x}$. The density field can be defined as:

$$\begin{aligned}\rho(\mathbf{r}, t) &= \rho_b(t) + \delta\rho(\mathbf{r}, t) \\ &= \rho_b(t)(1 + \delta(\mathbf{r}, t))\end{aligned} \tag{2.2}$$

Here ρ_b is the background density. This is independent of the spatial coordinates because it is the solution of the Friedmann equations. δ is defined as the density contrast and is equal to $\delta\rho/\rho_b$.

For any particle in the universe, its physical velocity is $\mathbf{u} = \dot{\mathbf{r}}$ where the overdot represents the total derivative in time. Thus

$$\begin{aligned}\mathbf{u} &= \dot{a}\mathbf{x} + a\dot{\mathbf{x}} \\ &= \dot{a}\mathbf{x} + v\end{aligned}$$

Here one can see the distinct components of velocity, the first simply being hubble flow while the second represents peculiar velocity. For such a particle, the kinetic energy is $mu^2/2$

$$\begin{aligned}T &= \frac{mu^2}{2} \\ &= \frac{m\dot{a}^2x^2 + ma^2\dot{x}^2 + ma\dot{a}\mathbf{x}.\dot{\mathbf{x}}}{2}\end{aligned}$$

The lagrangian $\mathcal{L} = mu^2/2 - m\phi'$ for the scalar potential ϕ'. One can simplify this by recalling that the equations of motion are invariant under the addition of a total derivative of a scalar to the lagrangian. Consider the scalar:

$$\begin{aligned}\Psi &= \frac{ma\dot{a}x^2}{2} \\ \frac{d\Psi}{dt} &= \frac{m\dot{a}^2x^2 + ma\ddot{a}x^2 + ma\dot{a}\mathbf{x}.\dot{\mathbf{x}}}{2}\end{aligned}$$

The lagrangian is changed to:

$$\begin{aligned}\mathcal{L}' &= \mathcal{L} - \frac{d\Psi}{dt} \\ &= \frac{ma^2\dot{x}^2 - ma\ddot{a}x^2}{2} - m\phi'\end{aligned}$$

Redefining the potential as $\phi = \phi' + a\ddot{a}x^2/2$

$$\mathcal{L}' = \frac{mv^2}{2} - m\phi \tag{2.3}$$

The Euler Lagrange equations describe the motion of the particles. While deriving them, one needs to keep in mind that the trajectories must be consistent with the Friedmann equations. Thus they serve as constraints and one must use Langrange multipliers suitably to obtain their trajectories.

2.2.2 The field equation

The gravitational field is defined by the Poisson equation in the Newtonian limit.

$$\nabla_r^2 \phi' = 4\pi G \rho(\mathbf{r}, t) \tag{2.4}$$

Since we're going to work in comoving coordinates, we need to suitably transform this equation. These are how the partial derivatives transform:

$$\begin{aligned} \nabla_r &= \frac{1}{a}\nabla_x \\ \frac{\partial}{\partial t}_r &= \frac{\partial}{\partial t}_x - H\mathbf{x}.\nabla_{\mathbf{x}} \end{aligned} \tag{2.5}$$

Thus the transformed field equation is:

$$\begin{aligned} \nabla_x^2 \phi' &= 4\pi G a^2 \rho \\ \nabla_x^2 \left[\phi - \frac{a\ddot{a}x^2}{2}\right] &= 4\pi G a^2 \rho \\ \nabla_x^2 \phi &= 4\pi G a^2 \rho + 3a\ddot{a} \end{aligned} \tag{2.6}$$

2.2.3 In a matter dominated universe

The form of the first Friedmann equation is much simplified if we assume that the universe is dominated by matter and that the curvature $1 - \Omega_0 = 0$, i.e. a spatially flat universe. This assumption is justified in the time after radiation domination and before dark energy domination. Since matter dominance covers a sizeable portion of the universe's history, this isn't a bad assumption at all. In this scenario, the first Friedmann equation reduces to $H^2 = H_0^2 \Omega_{m0}/a^3$. This implies:

$$\begin{aligned} \frac{\dot{a}^2}{a^2} a^3 &= constant \\ \dot{a}^2 a &= constant \\ 2a\dot{a}\ddot{a} + \dot{a}^3 &= 0 \\ \ddot{a} &= \frac{-\dot{a}^2}{2a} \end{aligned} \tag{2.7}$$

The field equation is suitably modified. Substituting 2.7 in 2.6, we get:

$$\begin{aligned}\nabla_x^2\phi &= 4\pi G a^2\rho - \frac{3}{2}\dot{a}^2 \\ &= 4\pi G a^2\rho - \frac{3}{2}\left(a^2 H_0^2\Omega_m\right) \\ &= 4\pi G a^2\rho - 4\pi G a^2\rho_b \\ \nabla_x^2\phi &= 4\pi G a^2\rho_b\delta\end{aligned} \tag{2.8}$$

2.2.4 The fluid equations

All the matter present in the universe will behave essentially like a fluid. Thus we can write the equation of continuity and the Euler equation for it.

$$\frac{\partial\rho}{\partial t}_r + \nabla_r.(\rho\mathbf{u}) = 0 \tag{2.9}$$

$$\frac{\partial\mathbf{u}}{\partial t}_r + (\mathbf{u}.\nabla_\mathbf{r})\,\mathbf{u} = -\frac{1}{\rho}\nabla_r P - \nabla_r\phi' \tag{2.10}$$

As before, we need to recast these equations in terms of comoving coordinates. Using 2.5, firstly we transform the equation of continuity:

$$\begin{aligned}\frac{\partial\rho}{\partial t}_x - H\mathbf{x}.\nabla_\mathbf{x}\rho + \frac{1}{a}\nabla_x(\rho\mathbf{u}) &= 0 \\ \frac{\partial\rho}{\partial t}_x - H\rho + \frac{1}{a}\nabla_x(\rho\dot{\mathbf{a}}\mathbf{x} + \mathbf{v}) &= 0 \\ \frac{\partial\rho}{\partial t}_x + 3H\rho + \frac{1}{a}\nabla_x(\rho\mathbf{v}) &= 0\end{aligned} \tag{2.11}$$

Then, the Euler equation:

$$\begin{aligned}\frac{\partial\mathbf{u}}{\partial t}_x - H\mathbf{x}.\nabla_\mathbf{x}\mathbf{u} + \frac{(\mathbf{u}.\nabla_\mathbf{x})\mathbf{u}}{a} &= -\left(\frac{\nabla_x P}{\rho a} + \frac{\nabla_x\phi'}{a}\right) \\ \ddot{a}\mathbf{u} + \frac{\partial\mathbf{v}}{\partial t}_x + \frac{(\mathbf{v}.\nabla_\mathbf{x})\mathbf{u}}{a} &= -\left(\frac{\nabla_x P}{\rho a} + \frac{\nabla_x\phi'}{a}\right) \\ \ddot{a}\mathbf{u} + \frac{\partial\mathbf{v}}{\partial t}_x + \frac{(\mathbf{v}.\nabla_\mathbf{x})(\dot{a}\mathbf{x} + \mathbf{v})}{a} &= -\left(\frac{\nabla_x P}{\rho a} + \frac{\nabla_x\phi'}{a}\right) \\ \ddot{a}\mathbf{u} + \frac{\partial\mathbf{v}}{\partial t}_x + H\mathbf{v} + \frac{(\mathbf{v}.\nabla_\mathbf{x})\mathbf{v}}{a} &= -\left(\frac{\nabla_x P}{\rho a} + \frac{\nabla_x\phi'}{a}\right) \\ \frac{\partial\mathbf{v}}{\partial t}_x + H\mathbf{v} + \frac{(\mathbf{v}.\nabla_\mathbf{x})\mathbf{v}}{a} &= -\left(\frac{\nabla_x P}{\rho a} + \frac{\nabla_x\phi}{a}\right)\end{aligned} \tag{2.12}$$

Notice the replacement of ϕ' by ϕ in the last step. Henceforth, since we're working exclusively in the comoving coordinates, we shall drop the subscripts. If we were to recast the equations in terms of the density contrast, we'd have, in index notation:

$$\begin{aligned} \frac{\partial \delta}{\partial t} + \frac{\partial_i \left[(1+\delta)v^i\right]}{a} &= 0 \\ \frac{\partial v^i}{\partial t} + Hv^i + \frac{v^j \partial_j v^i}{a} &= -\left(\frac{\partial^i P}{a\rho_b(1+\delta)} + \frac{\partial^i \phi}{a}\right) \end{aligned} \tag{2.13}$$

In obtaining the first equation, we have used the fact that in a matter dominated universe $\rho_b \propto a^{-3}$ and thus

$$\frac{\partial \rho_b}{\partial t} + 3H\rho_b = 0 \tag{2.14}$$

One can proceed with further simplification. Multiplying 2.11 by v^j and 2.12 with δ and adding the two, we get:

$$\partial_t(\rho v^i) + 4H\rho v^i + \frac{\partial_j(\rho v^j v^i)}{a} = -\frac{1}{a}(\partial^i P + \rho \partial^i \phi) \tag{2.15}$$

Here, we are switching to the short-hand notation for partial derivatives. The indices are representative of spatial coordinates while t stands for differentiation w.r.t. time. It is nice to note that this is an equation which describes the transfer of momentum per unit volume in the universe. In fact, if $4H\rho v^i$ is brought to the RHS, one can identify the RHS to be some sort of a source term while the LHS is a total derivative (there is a factor of $1/a$ extra but that is because we are working in terms of comoving coordinates). We can recast this in terms of the density contrast.

$$\partial_t[\rho_b(1+\delta)v^i] + 4H\rho_b(1+\delta)v^i + \frac{1}{a}[\rho_b(1+\delta)v^j v^i] = -\frac{1}{a}(\partial^i P + \rho_b(1+\delta)\partial^i \phi)$$

Using 2.14 and 2.13:

$$H(1+\delta)v^i + \partial_t[(1+\delta)v^i] - \partial_t \delta v^i + \frac{1}{a}(1+\delta)v^j \partial_j v^i = -\frac{1}{\rho_b a}(\partial^i P + \rho_b(1+\delta)\partial^i \phi)$$

We can now take its divergence and use 2.13 to obtain:

$$\partial_t^2 \delta + 2H\partial_t \delta = \frac{\nabla^2 P}{\rho_b a^2} + \frac{1}{a^2}\nabla.(1+\delta)\nabla\phi + \frac{1}{a^2}\partial_i \partial_j [(1+\delta)v^i v^j] \tag{2.16}$$

This is the exact equation of growth of density perturbations in a flat space, matter dominated universe in the Newtonian limit.

2.3 Linear perturbation theory: The Meszaros equation

From 2.16 if want to obtain the linear theory, we need to understand the order of different quantities. From the CMBR, we know the amplitude of the perturbations in the early universe were of the order of one part in a hundred thousand. Calling this quantity ϵ, we can see that $\delta \propto \epsilon$ in the leading order. This implies ϕ was also linear in the leading order. The peculiar velocities are also $\mathcal{O}(\epsilon)$. Thus in 2.16, if one were to collect term only up to a linear order in ϵ, one would get:

$$\partial_t \delta + \frac{\nabla.\mathbf{v}}{a} = 0$$
$$\partial_t^2 \delta + 2H\partial_t \delta = \frac{1}{a^2 \rho_b}(\nabla^2 P + \rho_b \nabla^2 \phi)$$

Substituting 2.8 in the second equation, we get the Meszaros equation:

$$\partial_t^2 \delta + 2H\partial_t \delta = \frac{1}{a^2}\frac{\nabla^2 P}{\rho_b} + 4\pi G \rho_b \delta \tag{2.17}$$

Now it is not possible to solve this in the most general case analytically. Therefore, we shall consider special cases where the solution is tractable.

2.3.1 Solutions to the Meszaros equation

Case 1: $P = 0$

For this section alone, we shall assume the over-dots represent partial derivatives in time. It doesn't really matter in the case of the Hubble parameter or the scale parameter as they are purely functions of time but the same cannot be said of density contrast.

It is particularly simple to solve the Meszaros equation in the scenario of the background pressure being zero. Let's closely examine the equation:

$$\partial_t^2 \delta + 2H\partial_t \delta = 4\pi G \rho_b \delta$$

Since it is a second order equation, there are two linearly independent solutions. Now, it is not easy to notice this but H itself turns out to be a solution to this equation. Before we verify this, we need to keep in mind the second Friedmann equation. In the pressure-less scenario, it is reduced to:

$$\frac{\ddot{a}}{a} = -\frac{4}{3}\pi G \rho_b$$

Now let us substitute H in the LHS of the Meszaros equation:

$$\begin{aligned}
&= \ddot{H} + 2H\dot{H} \\
&= \frac{\partial}{\partial t}\left(\frac{\ddot{a}}{a} - \frac{\dot{a}^2}{a^2}\right) + 2\frac{\dot{a}}{a}\left(\frac{\ddot{a}}{a} - \frac{\dot{a}^2}{a^2}\right) \\
&= \frac{\dddot{a}}{a} - \frac{\ddot{a}\dot{a}}{a^2} - \frac{2\dot{a}\ddot{a}}{a^2} + \frac{2\dot{a}^3}{a^3} + \frac{2\dot{a}\ddot{a}}{a^2} - \frac{2\dot{a}^3}{a^3} \\
&= \frac{\dddot{a}}{a} - \frac{\ddot{a}\dot{a}}{a^2} \\
&= \frac{\partial}{\partial t}\left(\frac{\ddot{a}}{a}\right) \\
&= -\frac{4}{3}\pi G\dot{\rho}_b \\
&= -\frac{4}{3}\pi G(-3H\rho_b) \\
&= 4\pi G\rho_b H = RHS
\end{aligned}$$

Now that one solution is obtained, we can obtain the other using the Wronskian. If D were the other solution,

$$\begin{aligned}
W &= \dot{H}D - \dot{D}H \\
\dot{W} &= \ddot{H}D - \ddot{D}H \\
&= D(4\pi G\rho_b H - 2H\dot{H}) - H(4\pi G\rho_b D - 2H\dot{D}) \\
&= 2HW \\
\Rightarrow W &= C/a^2 \\
\Rightarrow D &= -CH\int_0^t \frac{da}{a^3H^3}
\end{aligned} \tag{2.18}$$

Here C is a constant of integration. Note that we solved a partial differential equation as if it were an ordinary one. This implies C is really a function of space. However, it is nice to note whatever the initial spatial dependence of the density contrast, linear perturbation theory predicts it will be preserved in form and will only get scaled by a function of the scale factor. The general solution is of course, a linear combination of the two.

Case II: $P \neq 0$

In this case, we can expand the pressure to a linear order in density:

$$\begin{aligned} P &= P_b + \frac{\partial P}{\partial \rho}(\rho_b \delta) \\ &= P_b + c_s^2 \rho_b \delta \\ \Rightarrow \nabla^2 P &= c_s^2 \rho_b \nabla^2 \delta \end{aligned}$$

c_s being the speed of sound here. It is considered to be independent of spatial coordinates as a zeroth order approximation. Since δ is itself linear, we needn't consider the fluctuations in the speed of sound. Putting this in the Meszaros equation:

$$\partial_t^2 \delta + 2H\partial_t \delta = \frac{c_s^2}{a^2}\nabla^2 \delta + 4\pi G \rho_b \delta$$

This can be solved simply by the use of fourier transform from physical space to momentum space.

$$\partial_t^2 \tilde{\delta} + 2H\partial_t \tilde{\delta} = \tilde{\delta}\left(4\pi G\rho_b - c_s^2 \frac{k^2}{a^2}\right)$$

k being the wavevector modulus. This implies each mode evolves independently of the other. Linearity implies this sort of independence in the fourier space representation. This equation is now reduced in complexity and one can see the similarity between it and a damped harmonic oscillator. The key difference being the time dependence of the coefficient of $\partial_t \tilde{\delta}$. One would require numerical methods to get the exact solution. However, we can make guesses regarding the nature of the solution. Key to this lies in the coefficient of $\tilde{\delta}$. For the critical wavelength of

$$\lambda_J = \sqrt{\frac{\pi}{G\rho_b}} c_s \tag{2.19}$$

it would be zero and the solutions would be exponentially growing. This is called the Jean's length. It defines a length scale that determines whether or not a perturbation will grow. All wavelengths above this length scale will experience a growth and all below will oscillate and get damped in a universe with positive H. The time scale would of course depend on the value of H itself.

2.3.2 The peculiar velocity

Now that we have solved for the density contrast, the peculiar velocity can be solved for using the linearised form of the first equation of 2.13.

$$\partial_t \delta + \frac{\partial_i v^i}{a} = 0$$

Now δ can be written in terms of the potential as:

$$\delta = -\frac{\nabla^2 \phi}{4\pi G \rho_b a^2}$$

This implies:

$$\nabla.\mathbf{v} = \nabla.\left[a\partial_t\left(\frac{\nabla\phi}{4\pi G\rho_b a^2}\right)\right]$$
$$\Rightarrow \mathbf{v} = a\partial_t\left(\frac{\nabla\phi}{4\pi G\rho_b a^2}\right) + \mathbf{F} \text{ where } \nabla.\mathbf{F} = \mathbf{0}$$

In the regime of linear perturbation, $\mathbf{F}$ decays as $1/a$. This can be shown by considering the peculiar acceleration: $\mathbf{g} = d_t(a\mathbf{v})/a$. The total derivative of $\mathbf{v}$ can be replaced with a partial derivative in time because the term $(\mathbf{v}.\nabla)\mathbf{v}$ is second order in $\mathbf{v}$ and can be effectively neglected.

$$\mathbf{g} = \partial_t \mathbf{v} + H\mathbf{v} = -\frac{\nabla\phi}{a}$$

Now since $\mathbf{g}$ itself is curl-less, splitting the equation above into the divergence and divergence-free parts, we can say:

$$\partial_t(a\mathbf{F}) = 0$$

Thus the decay.

2.4 Non-linear perturbations: Spherical collapse

The spherically symmetric case is the easiest to solve for non-linearly. Consider matter at the boundary of a spherically symmetric, uniformly over-dense region characterised by a density contrast of δ. If the total mass in the spherical region is M, the gravitational acceleration experienced by it is:

$$\frac{d^2 r}{dt^2} = -\frac{GM}{r^2}$$

Integrating this once give us the statement of conservation of energy.

$$\frac{\dot{r}^2}{2} - \frac{GM}{r} = E \tag{2.20}$$

The behaviour of matter distribution depends on E. If E is negative, the region is gravitationally bound and if initially expanding, will come to a halt and subsequently contract eventually. If positive, the sphere continues expanding indefinitely.

To rephrase this condition of collapse, consider beginning at a time when the density contrast was small. In which case, $\dot{r}_i \approx H_i r_i$ (the peculiar velocities being very small). The subscript i here refers to initial conditions. The potential energy per unit mass at this instant is

$$U = -4\pi G\rho_b(1+\delta_i)r_i^2/3 = -H_i^2 r_i^2 \Omega_i(1+\delta_i)/2 = -K_i\Omega_i(1+\delta_i)$$

Where K_i is the initial kinetic energy per unit mass. Thus: $E = K_i\Omega_i(\Omega_i^{-1} - (1+\delta_i))$. The condition for collapse, $E < 0$ becomes: $\delta_i > \Omega_i^{-1} - 1$. In a closed or a flat universe where $\Omega \geq 1$, this is satisfied by any over-dense region. In an open universe, there exists a critical value above which such a condensation will occur.

Consider now, a spherical shell whose maximum radius is r_m. Thus,

$$E = -\frac{GM}{r_m} = -\frac{r_i}{r_m}K_i\Omega_i(1+\delta_i)$$

Or

$$\frac{r_m}{r_i} = \frac{1+\delta_i}{1+\delta_i-\Omega_i^{-1}}$$

The size of r_m in units of r_i would be very large if the overdensity were just larger than $\Omega_i^{-1} - 1$. This could mean a very long collapse time.

It is fairly straightforward to integrate 2.20, which we shall do now for the case of negative E. For the sake of clarity, let's say $E = -A$.

$$\dot{r} = \sqrt{\frac{2GM}{r} - 2A}$$
$$t - t_i = \int_{r_i}^{r} \frac{\sqrt{r'}dr'}{\sqrt{2GM - 2Ar'}}$$

After substituting $r' = (GM/A)\sin^2\theta'$ and integrating, we get:

$$t - t_i = \frac{GM}{A^{3/2}}\left[(2\theta - 2\theta_i) - (\sin 2\theta - \sin 2\theta_i)\right]$$

We have a parametric solution. This solution is periodic and one can fix the value of θ_i in terms of the initial radius. There are two free parameters, namely the energy and the initial density contrast. We can re-parametrise these equations in more convenient terms as follows:

$$r = X(1 - \cos\Theta), t + T = Y(\Theta - \sin\Theta), X^3 = GMY^2$$

This is just renaming the constants and setting $\Theta = 2\theta$. One can recognise this as the parametric equation for a cycloid.

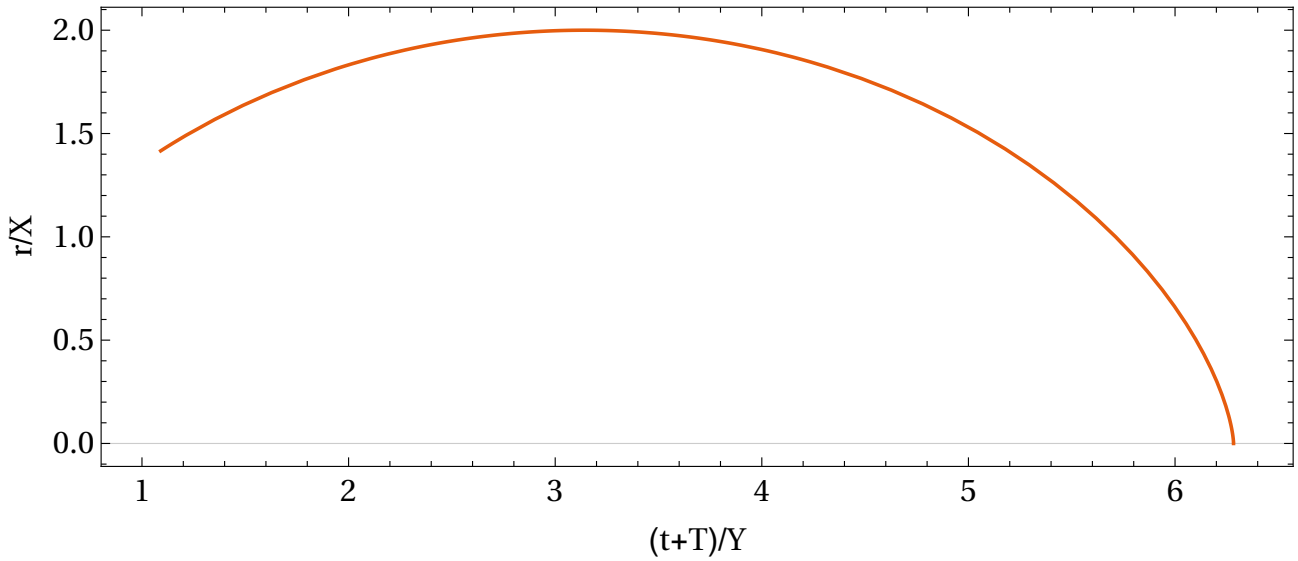

Figure 2.1: The temporal evolution of the radius of a spherically symmetric perturbation. The parameter Θ goes from an arbitrary initial point (2 in this case) to 2π. Of course, if Θ were to exceed that, this would periodically repeat. One needs to take into account the pressure experienced by matter at larger densities to effectively halt the gravitational collapse.

In these terms, the maximum radius would be $2X$ and thus

$$X = \frac{r_i}{2}\frac{1+\delta_i}{1+\delta_i-\Omega_i^{-1}}$$
$$Y = \frac{1+\delta_i}{2H_i\Omega_i^{1/2}(1+\delta_i-\Omega_i^{-1})^{3/2}}$$

2.4.1 Flat background universe

In this case, the equations are simplified on the account of $\Omega_i = 1$. Thus,

$$r = \frac{r_i}{2}\left(\frac{1+\delta_i}{\delta_i}\right)(1-\cos\Theta)$$
$$t + T = \frac{1}{2H_i}\frac{1+\delta_i}{\delta_i^{3/2}}(\Theta - \sin\Theta)$$

At $t = t_i$, $\cos\Theta_i = (1-\delta_i)/(1+\delta_i)$. Going by our assumption that $\delta_i \ll 1$, $\cos\Theta_i \approx 1 - 2\delta_i$. Or $\Theta_i^2 \approx 4\delta_i$. This means

$$H_i(t_i + T) = \frac{2}{3}(1+\delta_i)$$

Since the background universe in a matter dominated context obeys $H_i t_i = 2/3$, it follows that $T = 2\delta_i/3H_i$ or $T/t_i = \delta_i \ll 1$.

To understand the evolution of the density contrast, one must understand the evolution of the background density as well. In the matter dominated universe,

$$\begin{aligned} a \propto t^{2/3}; \rho_b &= \frac{1}{6\pi G t^2} \\ \therefore 1 + \delta = \frac{\rho}{\rho_b} &= \frac{3M}{4\pi X^3}\frac{6\pi G Y^2(\Theta - \sin\Theta)^2}{(1-\cos\Theta)^2} \\ \delta &= \frac{9(\Theta - \sin\Theta)^2}{2(1-\cos\Theta)^3} - 1 \end{aligned} \tag{2.21}$$

In the low Θ limit,

$$\begin{aligned} \delta &= \frac{9}{2}\frac{(\frac{\Theta^3}{3!} - \frac{\Theta^5}{5!} + \mathcal{O}(\Theta^7))^2}{(\frac{\Theta^2}{2!} - \frac{\Theta^4}{4!} + \mathcal{O}(\Theta^6))^3} - 1 \\ &= \left(1 - \frac{\Theta^2}{10} + \mathcal{O}(\Theta^4)\right)\left(1 + \frac{\Theta^2}{4} + \mathcal{O}(\Theta^4)\right) - 1 \\ &= \frac{3\Theta^2}{20} + \mathcal{O}(\Theta^4) \\ t &= \frac{Y\Theta^3}{6} + \mathcal{O}(\Theta^5) \\ \therefore \delta &\approx \frac{3}{20}\left(\frac{6t}{Y}\right)^{2/3} \end{aligned}$$

Since $H_i = 2/(3t_i)$ for a flat, matter dominated universe,

$$\delta = \delta_i\left[\frac{3}{5}\left(\frac{t}{t_i}\right)^{2/3}\right] \propto a$$

This is exactly what one would get if one were to pop $H = 2/(3t)$ in 2.18. Thus this is consistent with the linear solution in the case where there is no peculiar velocity.

$t/Y = 2\pi$ corresponds to the case when the spherical overdensity collapses to a single point. This put in the expression for δ in the linear limit yields $\delta \approx 1.69$. This defines a density scale for collapse.

2.4.2 Virialisation

It can be estimated that the density contrast at turn-around would be nearly 4.6. This clearly lies in the non-linear regime. Now of course, the overdensity won't collapse to a singularity because the assumption that the peculiar velocities are negligible would break down at some point and this would mean the matter would exert a counter-acting pressure and the matter would come to an equilibrium.

Equilibrium is reached via a process known as violent relaxation. This requires scattering of particles around small scale fluctuations and reach virial equilibrium in essentially the dynamical timescale, i.e. the time it takes for a particle to cross the spherical overdensity.

One can compute something called the virial velocity and virial radius, which are defined through the energy equation at virial equilibrium. When the perturbation reached its maximum radius, all energy was in the form of potential energy. At virial equilibrium,

$$\begin{aligned} K &= -\mathcal{E} \\ &= \frac{3GM^2}{5r_m} \\ 2K &= -U \\ Mv_{vir}^2 &= \frac{3GM}{5r_{vir}} \\ v_{vir} = \left(\frac{6GM}{5r_m}\right)^{1/2} &; r_{vir} = r_m/2 \end{aligned}$$

Once the system is virialised, its density doesn't change and the density contrast simply evolves due to the background expansion. The density is:

$$\rho_{coll} \approx 2^3 \rho_m = 8 \times 5.6 \rho_b(t_m) = 170 \rho_b(t_{coll})$$

Chapter 3

Halo mass function

3.1 Press-Schechter Formalism

In the conventional (by the standards of 1973) theory of cosmological perturbations, structures arose from condensations of mass from large lengthscales. That is, mass aggregates on larger length scales before gravitation took it further and made denser and denser objects: Large clouds condensed to small clouds and yet smaller ones. While this seems to explain the formation of large objects of the order of $10^{15}M$ and not on the scales of stars.

The way out of this proposed by Zeldovich [18] was to develop non-linear, pancake-like structures that then developed shocks and fragmented to form lumpier objects.

Press and Schechter in their 1973 paper [11] proposed a bottom up approach, citing the possibility of statistical fluctuations of matter density growing in size due to self gravitation. That is, starting from point masses, fluctuations could grow in size due to matter aggregating. What they obtained as a result was the distribution of objects with a mass in the range $[M, M + dM]$. This is called the *halo mass function*.

We saw in the previous section that density contrast of 1.69 or higher leads to gravitational collapse. Press-Schechter formalism predicts the fraction of the volume that has collapsed as:

$$f_{coll}(M(R), z) = \int_{\delta_c}^{\infty} \frac{2}{\sqrt{2\pi}\sigma(R, z)} e^{-\delta^2/2\sigma^2(R,z)} d\delta \tag{3.1}$$

This requires some explanation. Firstly, one must realise not all length-scales are similar when it comes to collapse statistics. The easiest way of seeing that is by considering a density

distribution and smoothing it over a window.

$$\delta(\mathbf{x}, R) = \int \delta(\mathbf{x}')W(\mathbf{x} - \mathbf{x}', R)d^3x$$

Many peaks that previously appeared over the critical value will now be below it or are smoothed out to form fewer peaks. Thus it appears as if more clumps will form on the lower lengthscale but they will be less massive. The process of smoothing is merely a convolution with a window function W. This is represented rather simply as a product in the Fourier space:

$$\delta(\mathbf{k}, R) = \delta(\mathbf{k})\tilde{W}(kR)$$

The functional dependence of $\tilde{W}$ on R is made explicit in the statement above. It appears specifically as a product kR. In 3.1, R is the radius of the smoothing window. M is the mass enclosed within.

$$M = \gamma_f \bar{\rho} R^3$$

Where $\bar{\rho}$ is the density averaged over the volume of the window and γ_f is a constant that depends on the shape of the window function. W is normalised such that its integral is 1 over the volume of integration. For example, $\gamma_f = 4\pi/3$ for a top hat profile (constant within the spherical window but 0 outside). The variance of the Gaussian integrand is a function of this radius and also the redshift of interest. Specifically, it is defined as the variance of the smoothed linear power spectrum.

$$\begin{aligned}\sigma^2 &= \frac{1}{(2\pi)^3}\int P_{lin}(k)\tilde{W}^2(kR)d^3k \\ &= \frac{1}{(2\pi)^2}\int P_{lin}(k)\tilde{W}^2(kR)k^2dk\end{aligned}$$

Of course, there is implicit dependence of redshift in P_{lin} and hence σ. Now one can define the window function in terms of either the radius or the mass enclosed. So in terms of mass, the variance can be written as:

$$\sigma_M^2 = \left\langle \left(\frac{M(\mathbf{x}, R) - \bar{M}}{\bar{M}} \right)^2 \right\rangle$$

Where the M is the density convolved with the window function and multiplied by the window volume. $\bar{M}$ is the aveagre of M over that volume. Thus, given a particular redshift and a particular window, the fraction of volume that collapses is given by 3.1. Now this expression needs to be examined more carefully.

1. Now it is highly dubious that the distribution of inhomogeneities is Gaussian. This is simply because $\delta > -1$. Even if the mean were high and one could *approximate* the distribution to be Gaussian, evolution under the influence of gravity would produce a lot of underdense regions and a significant tail of overdense regions.

2. The normalisation itself is questionable because of the factor of two in the numerator.

3. The proposed form of σ ignores non-linear effects. There is a huge disagreement in its value obtained from the linear power-spectrum as compared to the true non-linear one.

With all these points to be sceptic about, it is surprising that the formalism produces great numerical results regarding clustering. The factor of two in the normalisation was introduced as a fudge factor by Press and Schechter. Without this factor, the theory would predict that only half the mass of the universe would be locked up in haloes. There were more attempts to explain theoretically as to why the P-S formalism works so well. Another way of expressing 3.1 is in terms of number density of objects within a given mass range $[M, M + dM]$.

$$\begin{aligned}
\frac{dn}{dM} &= -\frac{\rho_m}{M}\frac{df_{coll}}{dM} \\
&= -\frac{\rho_m}{M}\frac{df_{coll}}{d\sigma}\frac{d\sigma}{dM} \\
&= -\frac{\rho_m}{M}\frac{d\sigma}{dM}\frac{d}{d\sigma}\int_{\delta_c}^{\infty}\frac{2}{\sqrt{2\pi}\sigma(R,z)}e^{-\delta^2/2\sigma^2(R,z)}d\delta \\
&= -\sqrt{\frac{2}{\pi}}\frac{\rho_m}{M}\frac{d\sigma}{dM}\frac{\delta_c}{\sigma^2}e^{\delta_c^2/2\sigma^2} \\
&= -\sqrt{\frac{2}{\pi}}\frac{\rho_m\delta_c R}{3M^2\sigma^2}\frac{d\sigma}{dR}e^{\delta_c^2/2\sigma^2}
\end{aligned} \tag{3.2}$$

Here ρ_m/M is the average number density of such objects. The negative signature essentially signifies the increasing rarity of more massive objects. The last equation uses the fact that $dM/dR = 3M/R$.

Now the critical density was calculated to be 1.69 for the case of the spherically symmetric model. If one were to perform numerical simulations and find out this value by keeping it a free parameter, it would turn out to be pretty close to 1.69.

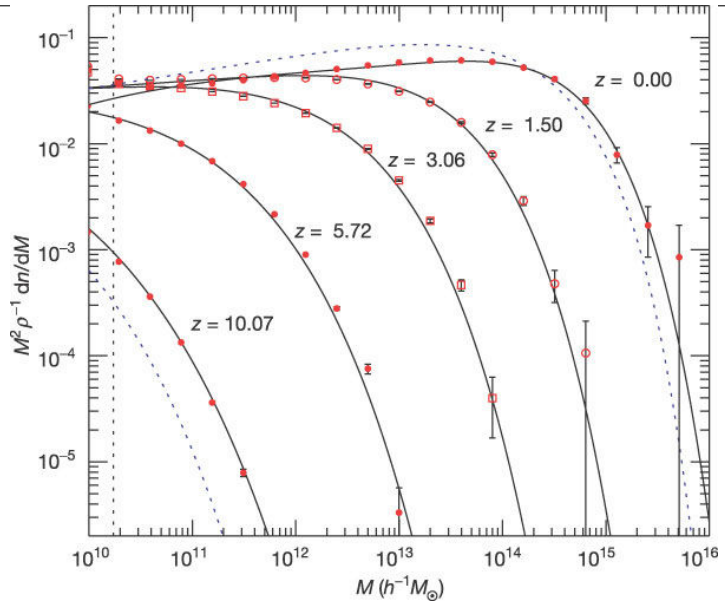

Figure 3.1: Results of the Millenium Simulation as compared to the PS halo mass function (in units of ρ_m/M^2). The solid lines are the best fit from Jenkins et al 2001 [5] and the dotted lines are from PS for redshifts 0 and 10.7. *source: Springel et al 2005[14]*

3.2 Beyond Press-Schechter

While the Press-Schechter formalism successfully explained the general trend of the halo mass function, the Millenium simulation showed the flaws in this approach. PS formalism doesn't quite match the observed distribution. As seen in Fig 3.1 The flaw in the formalism is assuming that the collapse is spherical. This is a highly unlikely scenario because peculiar velocities of particles in a small region that forms the halo needn't be isotropically distributed in phase space. One can have anisotropy within a halo and thus a better model would be one of ellipsoidal collapse. In order to account for these discrepancies, a general fitting function was proposed:

$$\frac{dN}{dM} = -f(\sigma)\frac{\rho_m}{M}\frac{d\log\sigma}{dM} \tag{3.3}$$

The PS halo mass function can be accommodate into this definition rather easily. The function $f(\sigma)$ is called a fitting function because it's form is proposed to best fit data from simulations/observations.

Sheth and Tormen in 1999 [13] proposed a form of the fitting function which, Tinker et

al. 2008 [17] parametrised in the following fashion:

$$f(\sigma) = A\left[\left(\frac{\sigma}{b}\right)^{-a} - 1\right] e^{-c/\sigma^2}$$

This is the form I will be using throughout this work. The values of the parameters (and their redshift evolution) are obtained from Tinker et al. 2008 for the mean halo overdensity of 200.

Chapter 4

Data and modelling

The metal ion absorption catalogue [19] has been produced using spectroscopic data from SDSS DR7. This catalogue includes 30,000 absorbers between redshifts 0.4 and 2.3. Zhu and Menard had created a search algorithm for finding the Mg II doublet of interest and thus were able to collect the vast number of absorbers in the SDSS DR7. The survey itself covered a significant fraction of the sky as shown in fig. 4.1 The survey was of course limited by the

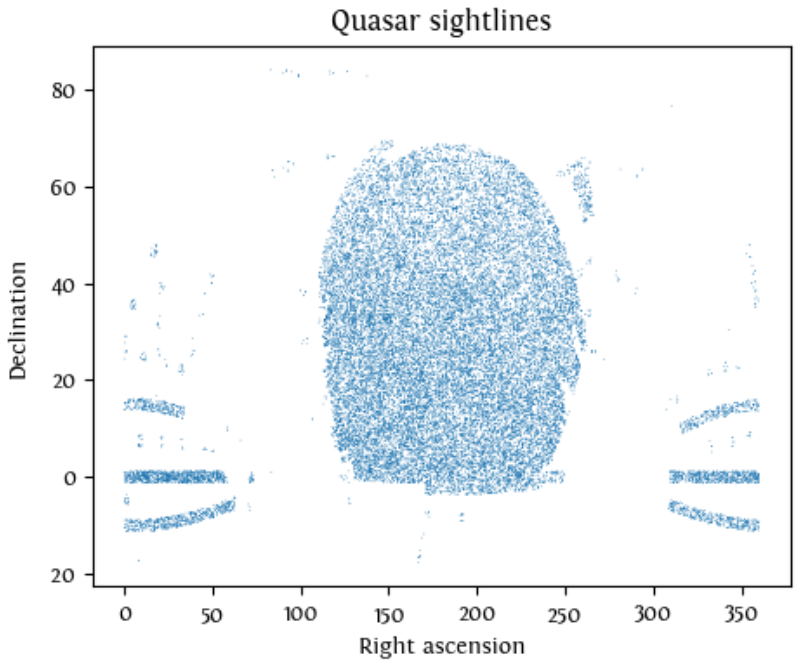

Figure 4.1: All sightlines in the sky included in the metal ion absorber catalogue produced by Zhu and Menard in 2013

capabilities of the telescope under use. Most importantly, it was limited by luminosity and

therefore dimmer sources were likely to be under represented in any sample produced observationally. This means the sample is not "complete" and therefore, to get the true number distribution, Zhu and Menard injected simulated absorption lines at various redshifts (dictated by the resolution of the spectrum) in the range 0.3 to 2.5. Then they checked whether the inserted lines could be detected or not and determined the fraction of lines detected for each value of rest equivalent width (of 279.6 nm line). This gave them an estimate of the underlying distribution of absorbers as opposed to the detected one.

4.1 Number density of absorbers in redshift space

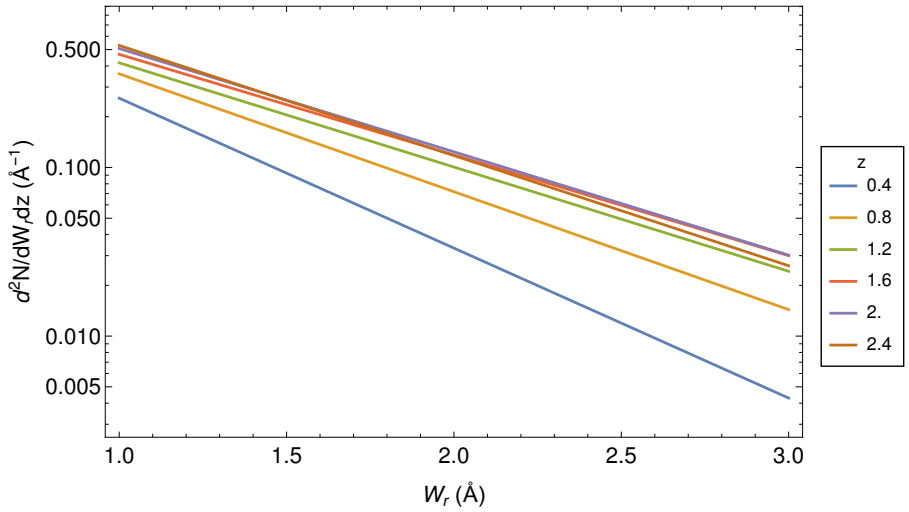

Figure 4.2: Zhu and Menard's fitting function for the number density of absorbers for some values of redshifts

According to Zhu and Menard's findings, the number density of absorbers $\partial^2 N/\partial W_r \partial z$ could be well explained by an empirical fit of the functional form proposed by them:

$$\frac{\partial^2 N}{\partial W_r \partial z}(z, W) = g(z) e^{-W/W^*(z)}$$
$$g(z) = g_0(1+z)^{\alpha_g}/(1+(z/z_g)^{\beta_g})$$
$$W^*(z) = W_0(1+z)^{\alpha_w}/(1+(z/z_w)^{\beta_w})$$

They have performed MC curve fits and identified the best fit values for the eight model parameters (fig 4.2) Notice the increase in number density until around redshift 1.5 and then a decrease. Thus the modelling that we do should be able to explain this specific redshift

evolution. The fits are reliable upto a rest equivalent width of 0.3 nm but beyond that the absorbers are few and thus the error bars are large.

Similiar studies previously have also incorporated bias estimates for absorber-galaxy cross-correlations [16]. In fact it is on the basis of these measurements that TC08 rejects their Classical model in favour of a Cold-Hot transition model that is inspires by hydrodynamical simulations which revealed formation of shock fronts in gas clouds in the CGM. However, for the sake of simplicity, I shall not delve into this model and see whether it suffices to consider a smooth gas distribution model alone.

4.2 Modelling the absorber distribution

Now that we are familiar with the theory regarding halo formation and distribution, we can go ahead with modelling the distribution of absorbers.

4.2.1 Dark matter halo profile

The first step in modelling is to first specify the distribution of dark matter in a halo. There have been numerous density profiles suggested over the years but going by TC08, I have taken the NFW profile [8]. It is a spherically symmetric, two-parameter model whose density function goes as:

$$\rho_{NFW}(r) = \frac{\rho_s}{(r/r_s)(1+r/r_s)^2} \tag{4.1}$$

There is a scale density ρ_s and an inner radius r_s that paramterise the density profile. Given a halo is defined to have a mean overdensity of Δ (usually 200), the mass enclosed is:

$$M = \Delta\rho_b \frac{4}{3}\pi r_\Delta^3$$

ρ_s can be expressed in terms of r_s because of the definition of r_Δ:

$$\bar{\rho} = \Delta\rho_b = \frac{3}{4\pi r_\Delta^3}\int_0^{r_\Delta} \rho(r) 4\pi r^2 dr = 3\rho_s \int_0^1 \frac{dx x^2}{cx(1+cx)^2}$$

$$\rho_s = \frac{\Delta}{3}\rho_b \frac{c^3}{\ln(1+c) - c/(1+c)}$$

Where $x = r/r_\Delta$ and $c = r_\Delta/r_s$ (the *concentration parameter*). The values of c are obtained by fitting simulated halos with the NFW profile. I am using the results from Dutton-Maccio 2014 [3] for the concentration-mass relation. This is done by using the open-source python module "halotools" (v0.5) [4].

4.2.2 Gas distribution model

Model description

Given a halo, one needs to populate it with gas. In the classical model described in TC08, gas is distributed in an NFW halo in a spherically symmetric fashion The gas has a finite

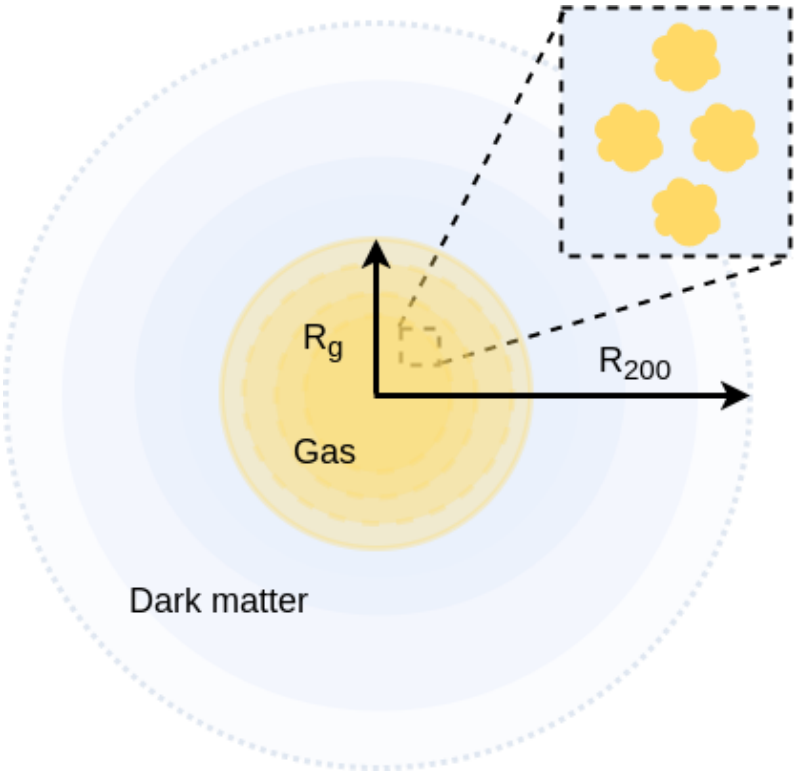

Figure 4.3: Distribution of gas in a halo according to the classical model proposed by Tinker and Chen 2008. There is a central gal halo in a dark matter halo. The gas halo is made of multiple clumps of gas. These are spatially distributed in a specific way and the dark matter halo has a1

extent R_g and is distributed in clumps. Each clump has a characteristic absorption strength and cross section. The number density of these absorbers is purely a function of radius and is given by:

$$\rho_g(r) = f_g G_0/(r^2 + a_h^2)$$

Where f_g is the gas fraction, a_h is the core radius and G_0 is a normalisation constant that is defined as:

$$G_0 = \frac{M(< R_g)/4\pi}{R_g - a_h \arctan(R_g/a_h)}$$

Where $M(< R_g)$ is the mass of dark matter enclosed in the gas halo. Integrating ρ_g over the volume of the gas halo gives the gas mass as $f_g M(< R_g)$. Initially, the gas radius is assumed to depend on mass as $80(M/10^{12}h^{-1}M_\odot)h^{-1}kPc$ as was done by Tinker and Chen.

Probability of absorption

For an absorption to be observed, there needs to be a line of sight that passes through a gas halo. The strength of absorption depends on the distance that light travels through a halo of given mass (fig 4.4). One integrates the gas density along the line of sight assuming each cloud of mass M_{cl} contributes a certain absorption cross section σ_{cl} and produces a width of W_0.

$$W_r(s|M) = W_0 \left[\frac{2\sigma_{cl}}{M_{cl}} \int_0^{\sqrt{R_g^2 - s^2}} \rho_g dl \right] = A_w(M) \frac{2G_0}{\sqrt{s^2 + a_h^2}} \arctan \sqrt{\frac{R_g^2 - s^2}{s^2 + a_h^2}}$$

Where $A_w = W_0 f_g \sigma_{cl}/M_{cl}$ clumps all the degenerate quantities into a single model parameter. This parameter is found to scale with mass as nearly a power law in TC08and I'm using the same scaling. First, we begin with the probability of a line of sight passing through the

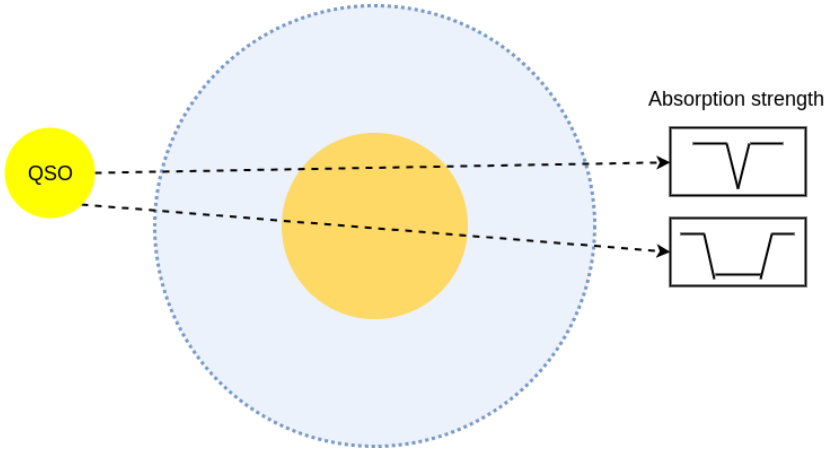

Figure 4.4: Absorption strength depends on the line of sight through a given halo (of a certain mass at a specific redshift). The rest equivalent width increases if the line of sight passes close to the centre as opposed to the fringe of the gas halo. Here the inner (orange, solid) circle represents the gas halo encapsulated by a dark matter halo (blue, dotted). To the right, are line profiles that one might obtain from the two lines of sight (dashed black arrows). Notice the one passing through the centre seems saturated.

gas halo at a radius r. Since the projected position of the LoS on a halo disk is uniformly

distributed, this is simply:

$$P(s|M) = \begin{cases} 2s/R_g & \text{if } s \leq R_g \\ 0 & \text{if } s > R_g \end{cases}$$

Now we need to determine the probability of a certain rest equivalent width W_r of absorption occurring from a halo of given mass. This simply depends on getting a certain combination of line of sight and a halo of required mass. Not all masses of halos contribute to absorption the same way. It depends on the covering fraction of the gas and also the amount of gas hosted by a halo. These being degenerate, they will be clubbed together in one parameter κ_g. Thus:

$$\begin{aligned} P(W_r|M)dW_r &= \kappa_g(M)P(s|M)ds \\ \therefore P(W_r|M) &= \kappa_g(M)P(s|M)\frac{ds}{dW_r} \\ &= \kappa_g \frac{2s}{R_g^2}\frac{ds}{dW_r} \end{aligned}$$

$s(W_r|M)$ is obtained by numerically inverting the relation for W_r. The exact form of κ_g is a unknown and Tinker and Chen use a non-parametric curve. They specify its value for four masses ($10^{10}, 10^{11.33}, 10^{12.66}, 10^{14}\ h^{-1}M_\odot$) and linearly interpolate in logarithmic space (i.e. it is a piecewise power-law). See fig. 4.5. This essentially conveys the fact that most halos associated with Mg II absorption are in the $10^{11} - 10^{13}h^{-1}M_\odot$ range.

Frequency distribution function

The number density of absorbers per unit rest equivalent width range and unit comoving path length is the integral over halo mass of the product of the halo mass function weighted by cross-section and probability of detecting an absorber with a certain rest equivalent width from a halo of given mass. i.e.

$$\begin{aligned} f(W_r) = \frac{d^2N}{dW_r dl} &= \int dM \frac{dn}{dM}\sigma_g(M)P(W_r|M) \\ &= \int dM \frac{dN}{dM}\pi R_g(M)^2 P(W_r|M) \end{aligned} \tag{4.2}$$

It is a simple matter of converting comoving distance to redshift. For the purposes of these calculations, I am assuming a cosmology consistent with Planck 13 data. The halo-mass function was incorporated using the "hmf" python module [7] and the corresponding fitting function ($f(\sigma)$) was taken from Tinker et al 2008 with their best fit parameter values.

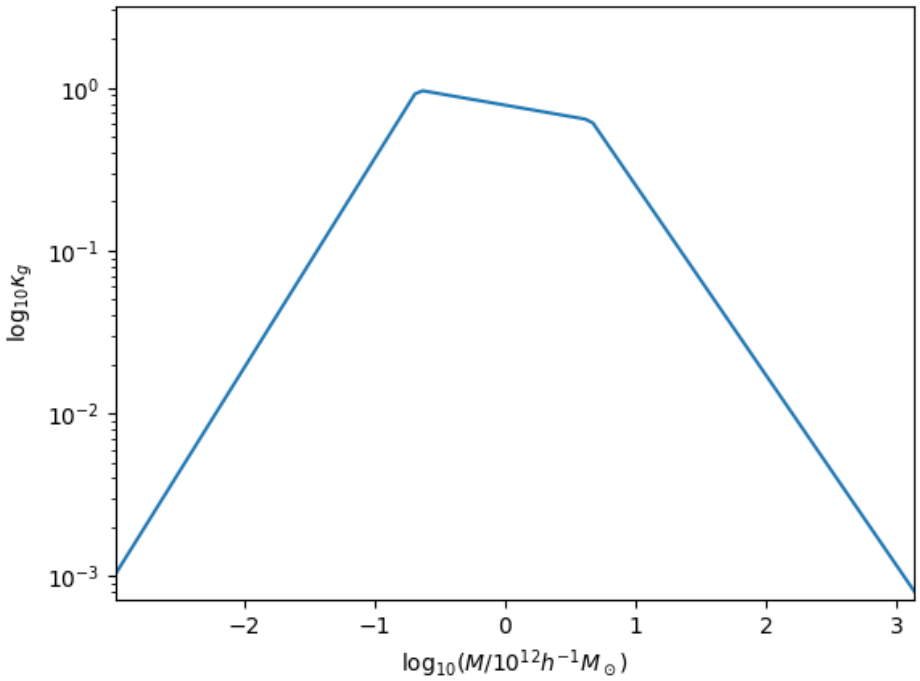

Figure 4.5: The form of κ_g chosen by Tinker and Chen

4.2.3 Results and Conclusions: Redshift dependence of κ_g

For the purpose of my analysis, I have taken all parameter values for the model from TC08. I have only changed one parameter A_{w0}, the value of A_w at $10^{12}h^{-1}M_\odot$ halos, from $13h$ nm cm^2/g to $9h$ nm cm^2/g so as to reproduce $f(W_r)$ as shown in TC08 at z = 0. This discrepancy might be because of the cosmological parameters taken and the concentration-mass relation for the NFW profile being different from TC08's. I intended to find the nature of κ_g for different values of redshift. For this purpose, I have assumed $kappa_g$ has a peaked shape, i.e. it has similar piecewise power-law shape as proposed by TC08 but I'm allowing the representative masses to vary instead of the value of κ_g. The values are fixed to 0.01 on the two ends and 1 in between the two inner values. This simplifies things in terms of curve fitting. I have to vary the four representative masses and find the combination that fits the observed number distribution well.

I have obtained forms of κ_g based on visual comparison of the model prediction versus the observed number density fig. 4.6. There does seem to be a shift towards lower masses

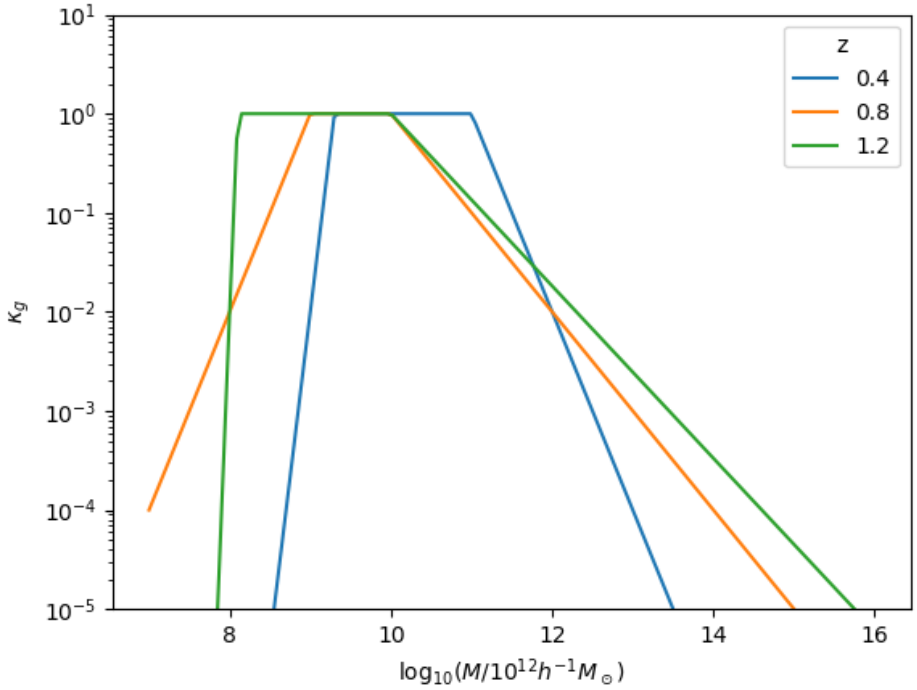

Figure 4.6: Forms of κ_g obtained from visual comparison of model prediction and observation for three redshifts

with increasing redshift up to 1.2. While this might give some idea of the halo-masses contributing to the observed distribution, it is obviously not rigorous by a long shot. I did attempt to fit it with the least-squares method but the error function seems to be rather complex in the parameter space under consideration (representative masses confined to the interval $10^8 - 10^{15}h^{-1}M_\odot$). What is required is a full fledged MCMC curve-fitting. I hope to be able to do this in the near future. What is necessary to be noted is that the visual fits become more elusive beyond z of around 1.2. This might imply a failure of the model in explaining the observations at such redshifts. It is possible that the Cold-Hot transition model put forth in TC08 as the better alternative may be able to fit the data better because of the additional parameters it brings into play.

Bibliography

[1] J. Bergeron. *Astronomy and Astrophysics*, (155):L8, 1986.

[2] C. Churchill et al. *Astrophysical Journal*, (543):577, 2000.

[3] A. A. Dutton and A. V. Maccio. *Monthly Notices of the Royal Astronomical Society*, (441):3359, 2014.

[4] A. Hearin et al. *Astronomical Journal*, (154):9, 2017.

[5] A. Jenkins et al. *Monthly notices of the Royal Astronomical Society*, (321):372, 2001.

[6] L. Lu and A. Wolfe. *Astronomical Journal*, (108):44, 1994.

[7] S. G. Murray, C. Power, and A. S. G. Robotham. *Astronomy and Computing*, (3):23, 2013.

[8] J. F. Navarro, C. S. Frenk, and S. D. M. White. *Astrophysical Journal*, (490):493, 1997.

[9] T. Padmanabhan. *Structure formation in the universe*. CUP, 1993.

[10] P. J. E. Peebles. *The Large-Scale Structure of the Universe*. PUP, 1980.

[11] W. Press and P. Schechter. *Astrophysical Journal*, (187):425, 1973.

[12] S. M. Rao, D. A. Turnshek, and D. B. Nestor. *Astrophysical Journal*, (636):610, 2006.

[13] R. K. Sheth and G. Tormen. *Monthly notices of the Royal Astronomical Society*, (308):119, 1999.

[14] V. Springel et al. *Nature*, (435):629, 2005.

[15] C. C. Steidel, M. Dickinson, and S. E. Persson. *Astrophysical Journal*, (437):L75, 1994.

[16] J. Tinker and H.-W. Chen. *Astrophysical Journal*, (679):1218, 2008.

[17] J. Tinker et al. *Astrophysical Journal*, (688):709, 2008.

[18] Y. B. Zeldovich. *Astrophysical Journal*, (5):84, 1970.

[19] G. Zhu and B. Menard. *Astrophysical Journal*, (770):130, 2013.